JOURNAL OF SOLID STATE CHEMISTRY 6, 136–150 (1973

The $Ba_{1-y}Sr_yMnO_{3-x}$ System

TAKI NEGAS

National Bureau of Standards, Washington, D.C. 20234

Received March 14, 1972

Subsolidus phase relations at ambient atmospheric pressure and elevated temperatures in the $Ba_{1-y}Sr_y$-MnO_{3-x} system were investigated by quenching, gravimetric, and X-ray diffraction methods. The system is not binary above ~1035°C because of reactions with atmospheric oxygen. The air isobar, $P_{O_2} = 0.2$ atm, was characterized at 1225, 1375, 1490, and 1610°C. Seven oxygen-deficient phases including a perovskite phase characterize the system. Their stability depends on the values of y and x in $Ba_{1-y}Sr_yMnO_{3-x}$. The cell dimensions of these phases expand as x increases at fixed y. These seven modifications can be retained in stoichiometric form by oxidation at lower temperatures.

Introduction

Phase relations in the $SrMnO_{3-x}$ and $BaMnO_{3-x}$ systems *in air* were investigated by Negas and Roth (*1–3*). Several phase transitions occur in these systems due to oxygen losses at elevated temperatures. Phases which are stabilized in these systems are *ideally* of the ABO_3-type (A = alkaline earth, B = transition metal). These feature mixed hexagonal and cubic-type stacking of close-packed AO_3 layers. A detailed discussion of the stacking of close-packed units and generated symmetry is provided in the "International Tables for X-ray Crystallography" (*4*). Katz and Ward (*5*) discuss some of the more relevant theoretical and experimental aspects of the stacking of AO_3 layers.

Low-temperature $SrMnO_3$, $a = 5.449$ Å, $c = 9.078$ Å, has the 4H (four-layer, hexagonal) structure (*1*, *2*, *6*, *7*) analogous to a $BaMnO_3$ form reported by Hardy (*8*). SrO_3 layers are stacked perpendicular to c in an ABAC sequence. The ratio of cubic to hexagonal-type layers (C/H) is 1.0. Oxygen octahedra containing Mn^{4+} are grouped into face-sharing pairs. These pairs are linked by corner-sharing within the cubically stacked A-layers. This structure remains stable in air, but with a small orthorhombic distortion, to approximately 1400°C and $SrMnO_{2.89}$ stoichiometry. At ~1400°C the 4H structure transforms to a distorted perovskite-type phase (100% cubic-type stacking) near $SrMnO_{2.74}$ stoichiometry. This phase is stable to about $SrMnO_{2.62}$ near a melting point at ~1740°C.

Low-temperature $BaMnO_3$, $a = 5.699$ Å, $c = 4.817$ Å (*3*) can be prepared in the 2H structure (*8*). BaO_3 layers are stacked in an AB sequence to yield 100% hexagonal-type stacking. Oxygen octahedra containing Mn^{4+} share faces in infinite strings parallel to c. With increasing temperature, oxygen losses generate a series of hexagonal phases characterized by a progressive increase in the C/H ratio. Except for the 2H and 4H modifications this series is illustrated by the idealized structures in Fig. 1. The reaction sequence *in air* is summarized by:

$$2H\ (C/H = 0) \xrightarrow{\sim 1150°C} 15R\ (C/H = 0.25)$$
$$\xrightarrow{\sim 1300°C} 8H\ (C/H = 0.33) \xrightarrow{\sim 1350°C}$$
$$6H\ (C/H = 0.50) \xrightarrow{\sim 1475°C} 10H\ (C/H = 0.67)$$
$$\xrightarrow{\sim 1550°C} 4H\ (C/H = 1.0).$$

The structures and stoichiometries of the above $BaMnO_{3-x}$ phases are discussed in detail elsewhere (*3*).

Phase transitions involving an increase in the amount of cubic stacking in ABO_3 compounds can be induced at elevated pressures. This is accomplished by the disruption of face-sharing octahedral sequences. The electrostatic repulsion

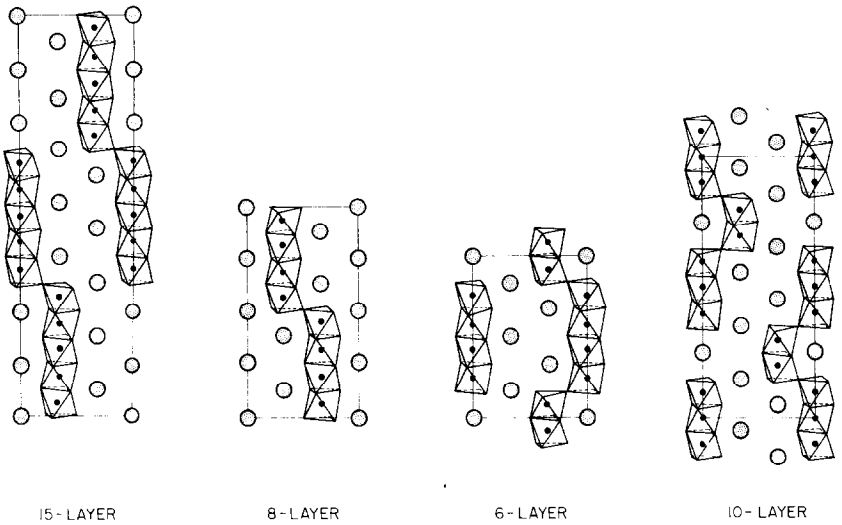

FIG. 1. Cation contents of the hexagonal (110) planes for the various hexagonal (H) and rhombohedral (R) phases which are stable in the $Ba_{1-y}Sr_yMnO_{3-x}$ system at ambient pressure. The 15R, 8H, 6H and 10H structures are idealized. Stable two-layer (2H), nine-layer (9R), four-layer (4H), and perovskite modifications are not shown. Large shaded circles are Ba and/or Sr cations. Small filled circles are Mn cations.

term increases as metal–metal distances for a given phase are progressively decreased. Ultimately, phase stabilization is possible by a transformation involving an increase in the amount of corner sharing. This phenomenon can be simulated by: (a) decreasing the effective size of the A cation for a given B transition metal; or (b) increasing the effective radius of the B metal for a given A cation. The series $Ba_{1-x}Sr_xRuO_3$ (*9*) illustrates (a). Method (b) is suggested by the pairs $SrMnO_3$(4H)–$SrRuO_3$ (perovskite) and $BaMnO_3$(2H)–$BaRuO_3$ (9R). As the effective radius increases from 0.54 to 0.62 Å (*10*) from Mn^{4+} through Ru^{4+}, shorter face-sharing distances are avoided by an increase in the C/H ratio. This results in an increase in the amount of corner-sharing.

The phase transitions observed in the $SrMnO_{3-x}$ and $BaMnO_{3-x}$ systems are reconciled with method (b) discussed above. Cubic stacking, however, is favored not by replacing the Mn^{4+} with a different, larger cation but by an increase in the effective radius of the Mn. This is accomplished by oxygen loss. Charge compensation is provided by the reduction of Mn^{4+} to the somewhat larger Mn^{3+} cation [$r = 0.58$ Å (*10*)].

The investigation of the system $Ba_{1-y}Sr_yMnO_{3-x}$ is concerned primarily with method (a). It was anticipated that additions of the smaller Sr^{2+} cation should favor a lowering in temperature of the stability fields of $BaMnO_{3-x}$ phases. Phases having progressively larger C/H ratios therefore should be stabilized at lower temperatures and higher Sr^{2+} contents.

Experimental Procedure

Weighed amounts of spectrographic grades of $SrCO_3$, $BaCO_3$, and Mn_3O_4 were hand mixed under acetone, packed in Au envelopes, and calcined in air at 800°C for 2 weeks followed by 8 weeks at 1000°C with periodic remixing. Calcined specimens in Pt tubes were equilibrated at selected temperatures and quenched in solid CO_2 or liquid N_2. Furnaces used and temperature control are described in (*2*) and (*3*).

Gravimetric data were obtained generally from 1.0–1.5 g specimens, which were previously equilibrated at a desired temperature and quenched. These specimens were weighed at room temperature, then heated in air to about 1000°C. The specimens were removed from the furnace after permitting enough time for any weight changes to occur. The specimens were then reweighed after cooling. Unless otherwise indicated, all measurements involve a weight gain from a high-temperature phase to a low-temperature oxidized phase.

X-ray powder patterns of specimens were made at room temperature using a diffractometer and Ni-filtered Cu radiation. The scanning rate was 1/4° 2θ/min. Interplanar d-spacings from

X-ray powder-diffraction measurements were used to compute unit-cell dimensions by a least-squares refinement computer program. Unit-cell dimensions are estimated to be accurate to within three standard deviations.

Experimental Results and Discussion

Subsolidus relations in the system $Ba_{1-y}Sr_y$-MnO_{3-x} at ambient atmospheric pressure are shown in Fig. 2, which was constructed from the quenching and gravimetric data in Table I. The unit-cell dimensions of 87 phases, listed in Table I, were also used in constructing the diagram. Phase relations for the limiting $BaMnO_{3-x}$ and $SrMnO_{3-x}$ systems were taken from (*1–3*). The system is not truly binary because of reactions with atmospheric oxygen. Figure 2 (upper portion) however, shows the position of the air isobar (x in $Ba_{1-y}Sr_yMnO_{3-x}$) at four

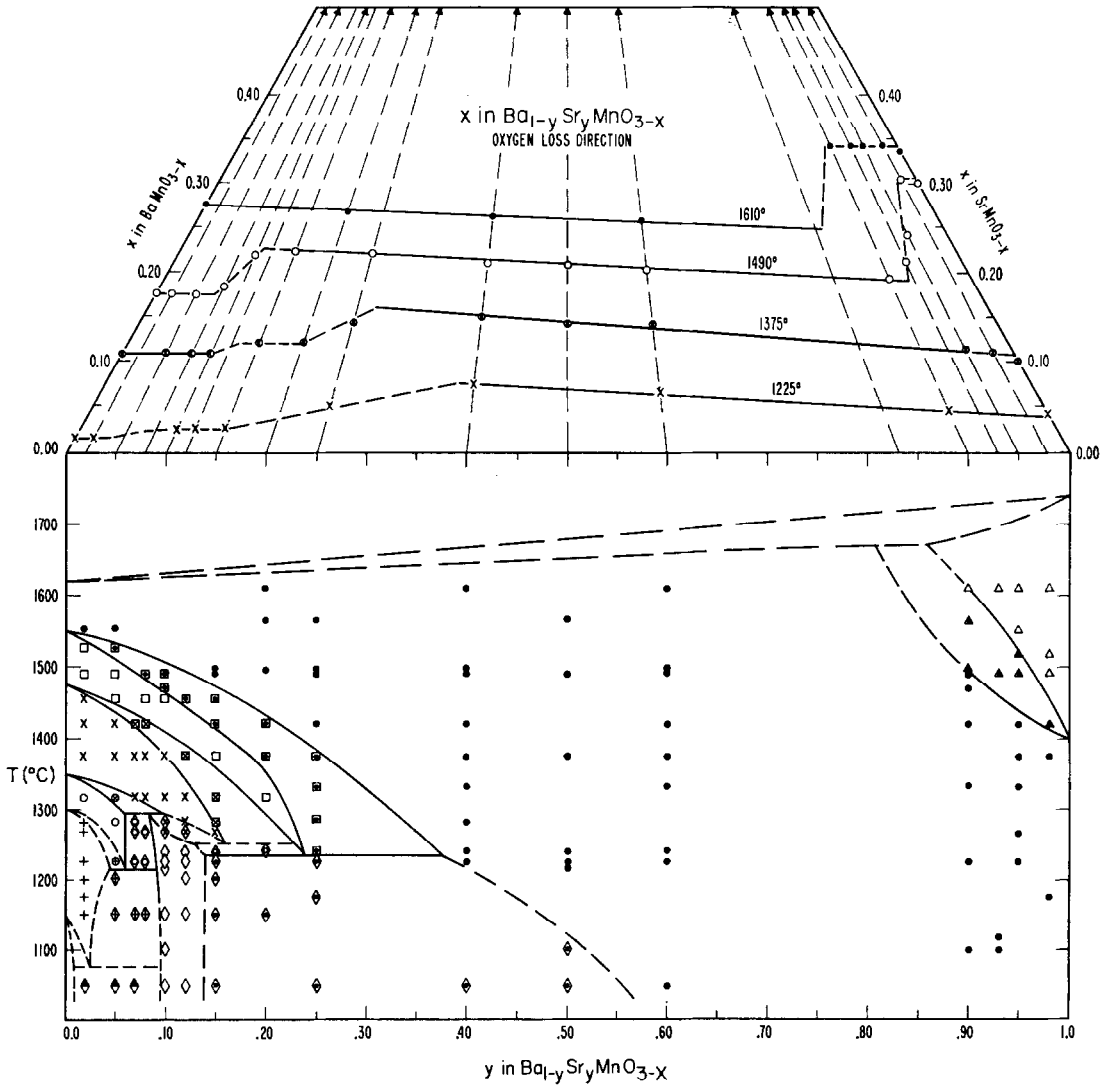

FIG. 2. Subsolidus phase relations at ambient atmospheric pressure in the system $Ba_{1-y}Sr_yMnO_{3-x}$. The system is not truly binary because of reactions with atmospheric oxygen. The location of the air isobar at four isotherms is depicted in the upper portion of the diagram. Data for the limiting $BaMnO_{3-x}$ ($y = 0$) and $SrMnO_{3-x}$ ($y = 1.0$) systems were taken from Negas et al. (*1–3*). Liquidus relations are inferred. Symbols in lower diagram: ⬘, 2H + 9R phases; ◇, 9R phase; +, 15R phase; ○, 8H phase; ×, 6H phase; □, 10H phase; ●, 4H phase; △, perovskite; plus combinations. Dashed lines with arrows, in upper portion of diagram, are lines of constant y and variable x in $Ba_{1-y}Sr_yMnO_{3-x}$.

Table I.

EXPERIMENTAL DATA FOR THE $Ba_{1-y}Sr_yMnO_{3-x}$ SYSTEM [1]

COMPOSITION	HEAT TREATMENT [2]		RESULTS [3]	COMPOSITION
y in $Ba_{1-y}Sr_yMnO_{3-x}$	Temp.(°C)	Time (day)	Phase Analysis and X-ray Powder Data	x in $Ba_{1-y}Sr_yMnO_{3-x}$ [4]
0.02	1050	95	2H + 9R	0.00
	1149	38	15R	
	1200	5	15R, reheat of 1050°C specimen	
	1225	27	15R	0.013
	1225	6	15R, reheat of 1225°, 27 days, specimen	0.016
	1267	25	15R	
	1280	32	15R	
	1317	37	8H	
	1373	15	6H, a = 5.674±0.001Å c = 14.056±0.002Å	
	1419	10	6H	
	1453	8	6H, a = 5.681±0.001Å c = 14.087±0.001Å	
	1490	3	10H, a = 5.675±0.001Å c = 23.373±0.008Å	0.178
			oxidized 1 day, 1000°C 10H, a = 5.650±0.001Å c = 23.173±0.002Å	
	1525	2	10H	
	1552	3	4H	
0.05	1050	95	2H + 9R	
	1120	10	15R + trace 9R	
	1149	38	15R + 9R	
	1200	5	15R + 9R; reheat of 1050°C specimen	
	1226	32	8H + 15R + trace 9R	
	1282	32	8H, reheat of a specimen initially heated 25 days, 1267°	
	1317	37	8H + 6H	
	1373	15	6H	
	1375	10	6H, a = 5.671±0.001Å c = 14.047±0.003Å	0.110
			oxidized 1 day, 1000°C 6H, a = 5.649±0.001Å c = 13.978±0.001Å	
	1385	20	6H, reheat of 1496° specimen	
	1419	10	6H	
	1453	8	10H, reheat of 1200° specimen	
	1457	6	10H	
	1490	3	10H, a = 5.672±0.001Å c = 23.346±0.006Å	
			oxidized 1 day, 1000° 10H, a = 5.645±0.001Å c = 23.164±0.002Å	0.177
	1496	3	10H	
	1525	2	10H + 4H	
	1552	3	4H	
			oxidized 1 hour, 800° 4H, a = 5.630±0.001Å c = 9.212±0.002Å	
0.07	1050	95	9R + 2H	
	1149	38	9R + 15R	
	1226	32	8H + 9R	
	1267	25	8H + 9R	
	1282	32	8H + 9R	
	1317	37	6H	
	1373	15	6H	
	1419	10	6H + 10H	
0.08	1149	38	9R + 15R	
	1175	31	9R + 15R + trace 6H; reheat of 1373° specimen	
	1226	32	9R + 8H	
	1267	25	9R + 8H	
	1317	37	6H	
	1373	15	6H, a = 5.664±0.001Å c = 14.036±0.002Å	
	1375	10	6H, a = 5.664±0.001Å c = 14.034±0.002Å	0.110
			oxidized 1 day, 1000° 6H, a = 5.645±0.001Å c = 13.976±0.002Å	
	1419	10	10H + 6H	
	1453	8	10H, a = 5.665±0.001Å c = 23.323±0.005Å	
	1490	3	10H + 4H 10H, a = 5.667±0.001Å c = 23.34±0.01Å	0.185
			oxidized 1 day, 1000° 10H + 4H 10H, a = 5.639±0.001Å c = 23.157±0.004Å	
0.10	1050	95	9R	0.00
	1100	28	9R	
	1120	5	9R + 10H; reheat of 1490° specimen; reaction is incomplete	
	1217	5	9R, reheat of 1100° specimen	
	1225	27	9R	0.023
	1225	33	9R, a = 5.649±0.001Å c = 20.930±0.002Å	0.021
	1226	14	9R, reheat of 1217° specimen	
	1237	32	9R	
	1267	25	6H + 9R + trace 8H	
	1286	5	6H + 9R	
	1317	37	6H	
	1322	5	6H, reheat of 1100° specimen	
	1373	15	6H, a = 5.661±0.001Å c = 14.031±0.002Å	
	1375	10	6H, a = 5.662±0.001Å c = 14.028±0.003Å	0.110
			oxidized 1 day, 1000° 6H, a = 5.642±0.001Å c = 13.975±0.001Å	
	1453	8	10H, a = 5.660±0.001Å c = 23.300±0.003Å	
	1457	6	10H	
	1470	2	10H + trace 4H	

TABLE I—*continued*

COMPOSITION	HEAT TREATMENT [2]		RESULTS [3]	COMPOSITION
y in $Ba_{1-y}Sr_yMnO_{3-x}$	Temp. (°C)	Time (day)	Phase Analysis and X-ray Powder Data	x in $Ba_{1-y}Sr_yMnO_{3-x}$ [4]
0.12	1050	95	9R	0.00
	1150	28	9R	
	1200	5	9R, reheat of 1050° specimen	
	1225	27	9R	0.022
	1225	33	9R	0.024
	1237	32	9R	
	1267	25	6H + 9R	
	1282	5	6H	
	1317	37	6H	
			oxidized 1 day, 1000°	
			6H, a = 5.640±0.001Å	
			c = 13.973±0.002Å	
	1373	15	10H + 6H	
	1453	8	10H + 4H	
			10H, a = 5.657±0.001Å	
			c = 23.284±0.004Å	
0.15	1050	95	9R + trace 4H	0.00
	1150	25	9R + trace 4H	
	1175	31	9R + 10H; reheat of 1373° specimen; incomplete reaction	
	1200	5	9R + trace 4H	
	1225	27	9R + trace 4H	0.021
	1225	33	9R + trace 4H; reheat of previous 1225° specimen	0.023
			9R, a = 5.638±0.001Å	
			c = 20.904±0.003Å	
	1237	32	9R + 10H	
	1267	25	6H	
			oxidized 1 day, 1000°	
			6H, a = 5.635±0.001Å	
			c = 13.972±0.002Å	
	1282	5	6H + trace 10H	
	1317	37	6H + 10H	
	1373	15	10H, a = 5.645±0.001Å	
			c = 23.22±0.01Å	
	1375	10	10H, a = 5.645±0.001Å	0.120
			c = 23.233±0.005Å	
			oxidized 1 day, 1000°	
			10H, a = 5.626±0.001Å	
			c = 23.133±0.002Å	
	1385	20	10H, reheat of 1496° specimen	
	1419	10	10H + 4H	
	1453	8	4H + 10H	
			4H, a = 5.641±0.001Å	
			c = 9.270±0.001Å	
	1490		4H	0.223
			oxidized 1 day, 1000°	
			4H, a = 5.614±0.001Å	
			c = 9.203±0.001Å	
	1496		4H, a = 5.646±0.001Å	
			c = 9.281±0.002Å	
0.20	1150	28	9R + 4H	
	1240	32	9R + 10H	
	1317	37	10H, a = 5.633±0.001Å	
			c = 23.193±0.003Å	
			oxidized 1 day, 1000°	
			10H, a = 5.616±0.001Å	
			c = 23.120±0.002Å	
	1375	15	10H + 4H	
			10H, a = 5.636±0.001Å	0.121
			c = 23.21±0.01Å	
	1419	10	4H + 10H	
			4H, a = 5.630±0.001Å	
			c = 9.258±0.003Å	
	1496	3	4H, a = 5.638±0.001Å	
			c = 9.270±0.001Å	
	1565	2	4H	
	1609	1	4H, a = 5.641±0.001Å	
			c = 9.280±0.001Å	0.266
	1610	1	4H, reheat of 1375° specimen	0.271
			oxidized 1 day, 1000°	
			4H, a = 5.605±0.001Å	
			c = 9.188±0.001Å	
0.25	1050	95	9R + 4H	
	1217	5	9R + 4H	
	1225	27	9R + 4H	0.051
	1225	33	9R + 4H	0.049
	1240	30	10H + 4H	
	1267	25	10H + 4H	
	1282	32	10H + 4H	
	1331	6	4H + 10H	
	1373	15	4H + 10H	
	1375	10	4H + 10H	0.143
	1419	10	4H, a = 5.621±0.001Å	
			c = 9.240±0.002Å	
			oxidized 1 day, 1000°	
			4H, a = 5.597±0.001Å	
			c = 9.182±0.001Å	
	1490	3	4H, a = 5.627±0.001Å	0.222
			c = 9.256±0.002Å	
			oxidized 1 day, 1000°	
			4H, a = 5.596±0.001Å	
			c = 9.183±0.001Å	
	1496	2	4H, a = 5.629±0.001Å	
			c = 9.262±0.001Å	
	1565	2	4H	

TABLE I—*continued*

COMPOSITION	HEAT TREATMENT [2]		RESULTS [3]	COMPOSITION
y in $Ba_{1-y}Sr_yMnO_{3-x}$	Temp. (°C)	Time (day)	Phase Analysis and X-ray Powder Data	x in $Ba_{1-y}Sr_yMnO_{3-x}$ [4]
0.40	1050	95	4H + 9R	
	1225	27	4H	0.076
	1225	32	4H, reheat of 1610° specimen a = 5.582±0.001Å c = 9.185±0.002Å	0.072
			oxidized 1 day, 1000° 4H, a = 5.571±0.001Å c = 9.160±0.002Å	
	1225	32	4H, reheat of 1375° specimen a = 5.581±0.001Å c = 9.186±0.002Å	0.070
	1226	32	4H, reheat of 1331° specimen a = 5.583±0.001Å c = 9.185±0.002Å	
	1241	25	4H	
	1282	5	4H	
	1331	6	4H, a = 5.591±0.001Å c = 9.206±0.001Å	
	1373	15	4H	0.150
	1375	10	4H	
			oxidized 1 day, 1000° 4H, a = 5.569±0.001Å c = 9.158±0.001Å	
	1419	10	4H, a = 5.598±0.001Å c = 9.221±0.001Å	
	1490	3	4H	0.211
	1496	2	4H, a = 5.604±0.001Å c = 9.234±0.001Å	
	1609	1	4H, a = 5.612±0.001Å c = 9.244±0.001Å	0.261
	1610	1	4H, a = 5.613±0.001Å c = 9.243±0.001Å	0.267
			oxidized 1 day, 1000° 4H, a = 5.569±0.001Å c = 9.156±0.002Å	
0.50	1050	95	4H + 9R	
	1100	28	4H + trace 9R	
	1149	38	4H	
	1217	5	4H	
	1226	32	4H, a = 5.564±0.001Å c = 9.169±0.002Å	
	1241	5	4H	
	1375	10	4H	0.141
			oxidized 1 day, 1000° 4H, a = 5.549±0.001Å c = 9.143±0.001Å	
	1490	3	4H, a = 5.583±0.001Å c = 9.210±0.002Å	0.210
			oxidized 1 hour, 1000° 4H, a = 5.550±0.001Å c = 9.144±0.001Å	
	1565	2	4H	
0.60	1050	95	4H	0.00
	1225		4H, a = 5.544±0.001Å c = 9.151±0.002Å	0.071
	1225		4H, reheat of 1610° specimen a = 5.543±0.001Å c = 9.152±0.002Å	0.065
			oxidized 1 day, 1000° 4H, a = 5.534±0.001Å c = 9.131±0.001Å	
	1225		4H, reheat of 1375° specimen	0.066
	1241	5	4H	
	1282	5	4H	
	1331	6	4H, a = 5.553±0.001Å c = 9.174±0.002Å	
	1375	10	4H, a = 5.555±0.001Å c = 9.176±0.003Å	0.142
			oxidized 1 hour, 1000° 4H, a = 5.532±0.001Å c = 9.132±0.001Å	
	1419	10	4H, a = 5.558±0.001Å c = 9.183±0.002Å	
	1490	3	4H	0.204
			oxidized 1 day, 1000° 4H, a = 5.533±0.001Å c = 9.130±0.001Å	
	1496	2	4H, a = 5.564±0.001Å c = 9.192±0.002Å	
	1609	1	4H, a = 5.572±0.001Å c = 9.210±0.002Å	0.258
	1610	1	4H	0.261
			oxidized 1 hour, 1000° 4H, a = 5.532±0.001Å c = 9.128±0.001Å	

TABLE I—*continued*

COMPOSITION	HEAT TREATMENT [2]		RESULTS [3]	COMPOSITION
y in $Ba_{1-y}Sr_yMnO_{3-x}$	Temp. (°C)	Time (day)	Phase Analysis and X-ray Powder Data	x in $Ba_{1-y}Sr_yMnO_{3-x}$ [4]
0.90	1100	28	4H	0.01
	1225	27	4H, a = 5.480±0.001Å c = 9.110±0.001Å	0.047
	1225	32	4H, reheat of 1610° specimen	0.045
			oxidized 1 day, 1000°	
			4H, a = 5.472±0.001Å c = 9.096±0.001Å	
	1331	6	a = 5.488±0.001Å c = 9.120±0.001Å	
	1419	10	a = 5.496±0.001Å c = 9.131±0.001Å	
	1470	2	4H	
	1490	3	4H	0.194
	1496	2	4H + P 4H, a = 5.502±0.001Å c = 9.134±0.001Å	
	1565	2	P + 4H	
	1610	1	P, a = 3.8497±0.0002Å	0.342
			oxidized 10 min, 400°	
			P, a = 3.8185±0.0002Å	
0.93	1100	28	4H	0.01
	1385	20	4H, reheat of 1490° specimen	
	1490	3	4H + P 4H, a = 5.494±0.001Å c = 9.125±0.001Å	0.212
	1610	1	P, a = 3.8461 0.0002Å	0.342
			oxidized 15 min, 400°	
			P, a = 3.8128±0.0003Å	
0.95	1175	31	4H, reheat of 1610° specimen	
	1226	32	4H, a = 5.470±0.001Å c = 9.102±0.001Å	
			oxidized 1 hour, 1000°	
			4H, a = 5.462±0.001Å c = 9.087±0.001Å	
	1241	5	4H	
	1331	6	4H, a = 5.478±0.001Å c = 9.112±0.001Å	
	1375	10	4H	0.113
			oxidized 1 hour, 1000°	
			4H, a = 5.461±0.001Å c = 9.088±0.001Å	
	1415	10	4H	
	1419	10	4H, a = 5.484±0.001Å c = 9.117±0.001Å	
	1490	3	P + 4H	0.243
	1515	3	P + 4H	
	1552	3	P, distorted, poorly crystalline	
	1610	1	P, distorted, poorly crystalline	0.342
			oxidized 1/2 hour, 400°	
			P, a = 3.8110±0.0002Å	
0.98	1175	31	4H, reheat of 1515° specimen	
	1375	10	4H	0.110
	1419	10	4H + P 4H, a = 5.475±0.001Å c = 9.110±0.002Å	
	1490	3	P, distorted, poorly crystalline	0.305
			oxidized 15 min, 400°	
			P, a = 3.8079±0.0002Å	
	1515	3	P, distorted, poorly crystalline	
	1610	1	P, distorted, poorly crystalline	0.342
			oxidized 1/2 hour, 400°	
			P, a = 3.8080±0.0002Å	

[1] Phase relations are for ambient pressure. See ref. (2,3) for data involving the limiting $BaMnO_{3-x}$ and $SrMnO_{3-x}$ systems.

[2] Does not include prior calcining.

[3] Phases were identified by powder x-ray diffraction at room temperature. H = hexagonal; R = rhombohedral, referred to hexagonal axes. The number preceeding H or R is the number of $(BaSr)O_3$ layers per unit cell (see text). P = perovskite

[4] Determined by oxidizing specimens at 1000° or 400°C in air.

isotherms. It must be used in conjunction with the lower portion of the figure which depicts phase relations only as a function of temperature and cation content. Liquidus relations are inferred.

The air isobar coincides with the $BaMnO_3$–$SrMnO_3$ join only below ~1035°C where the system is binary. Solid solutions are therefore stoichiometric with respect to anion content below 1035°C. Anion losses are evident above 1035°C and for every temperature the air isobar exists within the $Ba_{1-y}Sr_yMnO_{3-x}$ system with $0 < x < 0.4$ and $0 \leqslant y \leqslant 1$. At fixed temperature, x remains relatively constant while y remains within a one-phase field. Two-phase areas between solvus curves are characterized by an abrupt change in the slope of the isobar. This indicates that phase transitions are not gradational but rather involve a rapid variation of x, especially at temperatures >1225°C. At 1490°C, for example, the 10H phase is stable with $0 \leqslant y < 0.07$, while x remains essentially constant near 0.18. Transition to the 4H modification occurs between $y \approx 0.07$–0.12 as x rapidly increases to near 0.22. Similarly, the 4H to perovskite transition at 1490°C is associated with a $\Delta x \approx 0.10$.

It was considered unfeasible to demonstrate reversibility for every possible reaction shown in Fig. 2. Most phases or phase assemblages, therefore, were obtained by heating specimens prepared at lower temperatures. A number of reactions, however, were tested for reversibility as noted in Table I. Reversibility of phases in the limiting $BaMnO_{3-x}$ and $SrMnO_{3-x}$ systems is discussed in (*2*) and (*3*). Generally, reverse reactions are very sluggish, particularly at temperatures <1150°C. Single phase 15R and 8H phases will not transform to the appropriate phase(s) by reheating within a lower temperature-stability field. Reactions are so sluggish that at <1000°C it is possible to obtain stoichiometric forms of high-temperature, reduced phases. Weight increases associated with the general reaction,

$$Ba_{1-y}Sr_yMnO_{3-x} + xO \xrightarrow{<1000°C} Ba_{1-y}Sr_yMnO_3,$$

can be measured as "chemical equilibrium" is established rapidly within a few minutes or a few hours depending on the value of y. Transformation to the pertinent phase(s) at 1000°C ("crystallographic equilibrium") does not occur for most values of y within at least 1 month. Chemical and crystallographic equilibrium for the perovskite → 4H phase transition is easily accomplished at 1000°C within a few days. As in the $SrMnO_{3-x}$ system, however, reduced perovskites can be oxidized, without crystallographic transformation to the 4H phase, at temperatures <500°C. The rapid, low-temperature oxidation of reduced phases will be discussed in greater detail.

As anticipated, the temperature stability fields of the phases observed in the $BaMnO_{3-x}$ system are lowered by the addition of Sr^{+2} cations. The single phase regions converge and transform in reactions of the eutectoid- and peritectoid-type. It is evident that, at constant temperature, increased amounts of the smaller Sr^{2+} cation stabilize phases with progressively greater C/H ratios. The reduction process, however, is simultaneously competitive above ~1035°C. Phases with larger C/H ratios are stabilized as x increases at a fixed value of y.

Excluding those reduced phases which can be rapidly reoxidized without crystallographic change, only the 2H, 4H, and 9R (to be discussed) forms are stable with stoichiometric configurations. A 6H form analogous to $BaTiO_3$ (*11*) was not prepared in reduced or stoichiometric form. Syono et al. (*6*), and Chamberland et al. (*7*), however, prepared stoichiometric 6H $SrMnO_3$ at elevated pressures.

The 2H, 15R, and 8H Modifications

The stacking sequences with the smallest C/H ratios are stable with small values of x, generally <0.05, as in the $BaMnO_{3-x}$ system. Similarly, they can tolerate only small amounts of Sr^{2+} in solid solution. The 2H form, for example, accommodates $y < 0.02$ as suggested by the two-phase field, 2H + 9R, at $y = 0.02$ and 1050°C. The 15R and 8H forms accommodate $y < 0.05$ and $y < 0.06$, respectively. Since additions of the smaller Sr^{2+} cation simulate a pressure increase as previously discussed, the 2H, 15R, and 8H forms of stoichiometric $BaMnO_3$ must have very limited pressure–temperature stability fields.

The 9R Modification

A 9R phase could not be prepared in pure form in the limiting $BaMnO_{3-x}$ system (*3*), although Chamberland et al. (*7*) and Syono et al. (*6*) prepared the stoichiometric phase at elevated pressures. This form is isostructural with $BaRuO_3$ (*12*) which has an ABABCBCAC stacking sequence and a C/H = 0.50. Oxygen

octahedra containing Ru^{4+} are in strings of three which share faces. The strings are linked by corner sharing. Single phase 9R was prepared below 1300°C with $0.09 < y < 0.14$ and $0 \leqslant x < 0.03$. The stability of the 9R form with additions of $SrMnO_3$ in $BaMnO_3$ is in accord with the pressure work of (*6*) and (*7*) using the $BaMnO_3$ end member. The X-ray powder pattern for the 9R form prepared at 1225°C from the $y = 0.10$ composition is given in Table II. It is indexed on the basis of a hexagonal cell with $a = 5.649$ Å and $c = 20.930$ Å. Syono et al. (*6*) report $a = 5.667$ Å and $c = 20.948$ Å for the stoichiometric $BaMnO_3$ end member.

TABLE II

X-RAY POWDER DATA FOR THE 9R PHASE[a]

d_{obs}	d_{calc}	$h\,k\,l$[b]	I_{obs}
3.570	3.574	1 0 4	31
3.180	3.181	0 1 5	46
2.823	2.825	1 1 0	100
2.551	2.551	1 0 7	15
2.430	2.430	0 2 1	4
2.384	2.382	2 0 2	2[c]
2.326	2.326	0 0 9	15
2.307	2.307	0 1 8	17
2 216	2.216	0 2 4	30
2.112	2.112	2 0 5	40
1.9240	1.9243	1, 0, 10	9
1.8934	1.8933	0 2 7	8
1.7956	1.7953	1 1 9	6
1.7866	1.7868	2 0 8	12
1.7431	1.7435	2 1 4	7
1.6915	1.6915	1 2 5	16
1.6311	1.6308	3 0 0	18
1.5908	1.5903	0, 2, 10	8
1.5730	1.5727	2 1 7	8
1.5290	1.5293	1, 0, 13	6
1.5100	1.5100	1 2 8	7
1.4297	1.4297	0, 1, 14	5
1.4122	1.4123	2 2 0	17
1.3861	1.3858	2, 1, 10	7
1.3456	1.3456	3 1 2	6
1.3351	1.3352	3 0 9	3
1.3133	1.3135	1 3 4	5
1.2907	1.2908	3 1 5	8
1.2758	1.2756	2, 0, 14	5

[a] Nine-layer, rhombohedral, phase prepared at 1225°C in air. Composition is $Ba_{1-y}Sr_yMnO_{3-x}$ with $y = 0.10$ and $x \approx 0.02$.

[b] Indexed on the basis of a hexagonal cell with $a = 5.649 \pm 0.001$ Å, $c = 20.930 \pm 0.002$ Å.

[c] Broad.

The 6H and 10H Modifications

The stability fields of the 6H and 10H forms observed in the $BaMnO_{3-x}$ system extend into the $Ba_{1-y}Sr_yMnO_{3-x}$ system to at least $y = 0.15$ and $y = 0.20$, respectively. Cell parameters of the 6H form at constant y expand as x increases with increasing temperature. The linear variation of cell parameters with y (in $Ba_{1-y}Sr_yMnO_{3-x}$) of 6H forms quenched from 1375°C is shown in Fig. 3. It is possible to oxidize the reduced 6H phases at <1000°C in air. Crystallographic transitions are retarded at such low temperatures. The effects of the oxidation process are illustrated by the portions of X-ray diffraction powder patterns in Fig. 4 (a, b). A typical 6H phase prepared at 1375°C with $y = 0.05$ and $x = 0.11$ is shown in Fig. 4a. The pattern is characterized by a broadening of diffraction maxima. Figure 4b is the corresponding spectrum of the 6H phase oxidized to $x \approx 0$. The pattern is of excellent quality and maxima are shifted to larger 2θ values indicating a contraction of the cell parameters. This cell contraction is also depicted for other 6H phases in Fig. 3. Parameters for the phases at $y = 0.12$ and 0.15 were calculated from the X-ray patterns of oxidized specimens initially prepared in reduced form at 1317 and 1267°C (see Fig. 2). Figures 3 and 4 clearly demonstrate the differences between the partially and totally filled anion lattices.

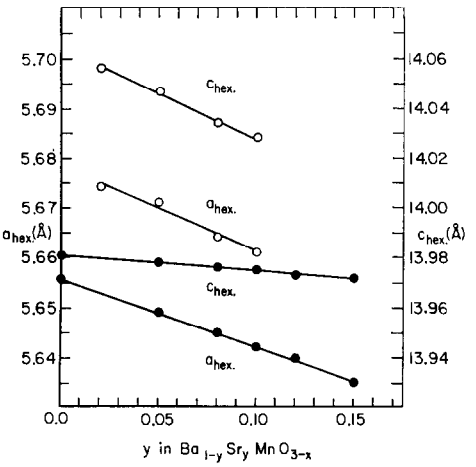

FIG. 3. Variation of the hexagonal cell dimensions for 6H modifications in the $Ba_{1-y}Sr_yMnO_{3-x}$ system. Open circles are the parameters of oxygen-deficient ($x \approx 0.11$) 6H phases prepared at 1375°C and quenched to room temperature. Closed circles are the parameters at room temperature of 6H phases which were initially reduced then oxidized ($x \approx 0$) at 1000°C.

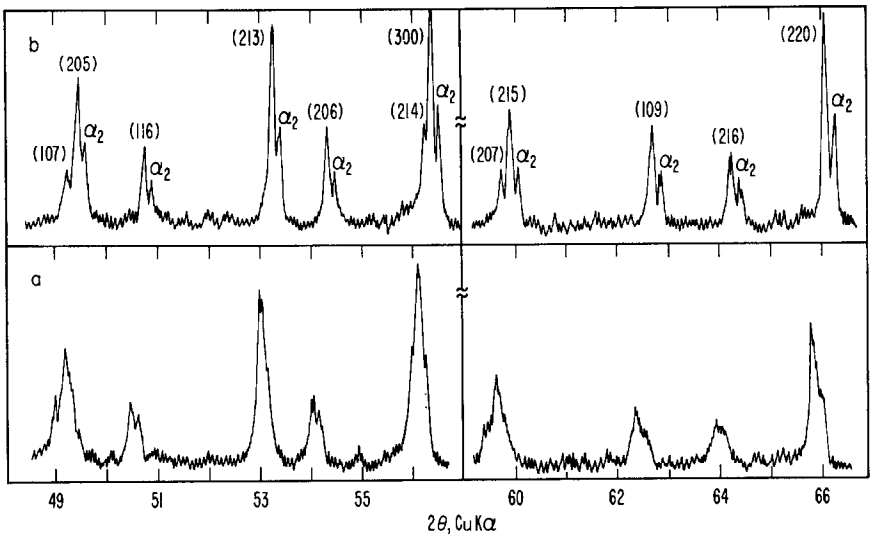

FIG. 4. Portions of the X-ray diffraction powder patterns at room temperature of a typical 6H phase prepared at 1375°C in air with $y = 0.05$ in $Ba_{1-y}Sr_yMnO_{3-x}$. The oxygen-deficient, $x \approx 0.11$, form is shown in (a). The pattern in (b) is obtained after the 6H phase in (a) is oxidized ($x \approx 0$) at 1000°C. The segmented vertical line is a discontinuity along the 2θ scale.

The 10H phase shows similar cell expansions and contractions with variable x and y. Figure 5 (a, b) illustrates portions of the X-ray powder patterns of a typical, reduced 10H form which was oxidized at 1000°C. The oxidation process clearly yields a phase characterized by a high-quality X-ray diffraction pattern and smaller cell parameters. A linear variation of cell parameters with y for oxidized 10H phases is evident in Fig. 6. Reduced 10H forms have significantly larger cell dimensions as shown in Table I. Parameters for the phases at $y = 0.15$ and

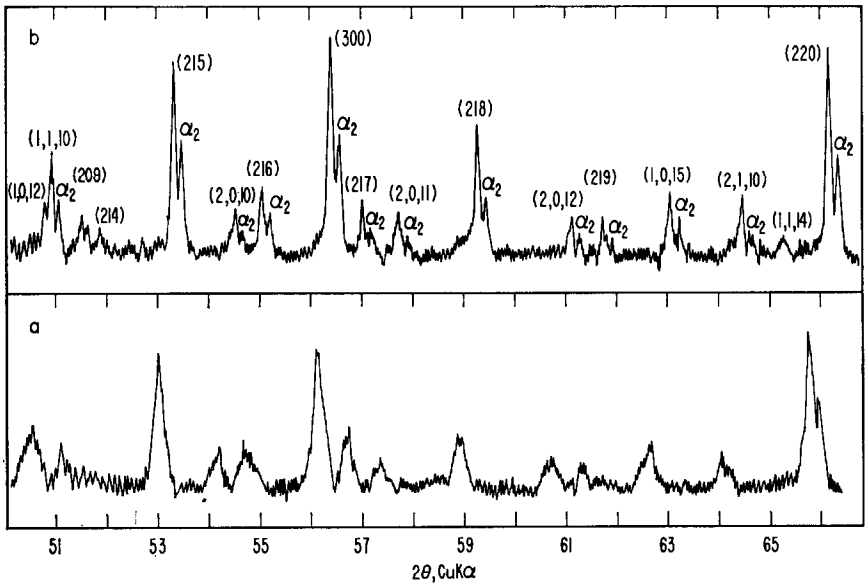

FIG. 5. Portions of the X-ray diffraction powder patterns at room temperature of a typical 10H phase prepared at 1490°C in air with $y = 0.05$ in $Ba_{1-y}Sr_yMnO_{3-x}$. The oxygen-deficient, $x \approx 0.18$, form is shown in (a). The pattern in (b) is obtained after the 10H phase in (a) is oxidized ($x \approx 0$) at 1000°C.

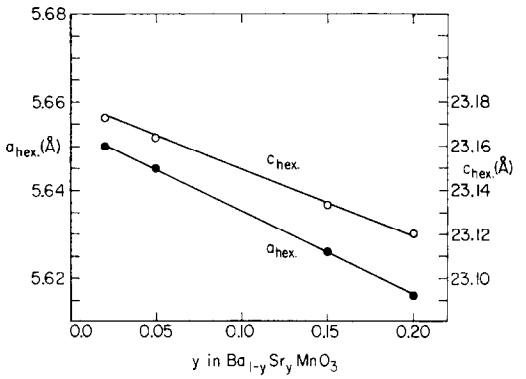

FIG. 6. Variation of the hexagonal cell dimensions of 10H phases in the $Ba_{1-y}Sr_yMnO_{3-x}$ system. Specimens were prepared initially as oxygen-deficient phases within the one phase 10H field in Fig. 2. See Table I for the cell dimensions of the reduced 10H forms. These were then oxidized ($x \approx 0$) at 1000°C.

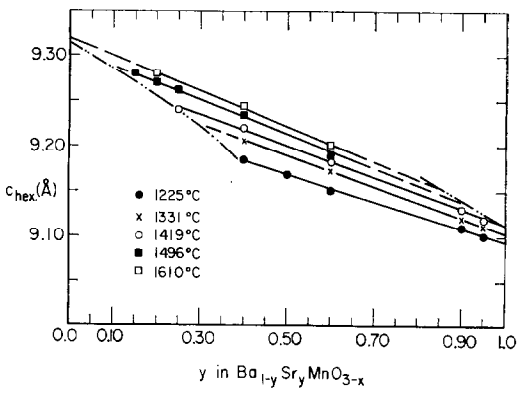

FIG. 7. Variation of the hexagonal c-axis dimension determined at room temperature of 4H modifications prepared in air at five temperatures in the $Ba_{1-y}Sr_yMnO_{3-x}$ system. The dash-dot lines delimit the stability field of the 4H phase between 1225–1610°C (see Fig. 2).

$y = 0.20$ were calculated from the X-ray patterns of oxidized specimens initially prepared in reduced form at 1375 and 1317°C, respectively (see Fig. 2).

The 4H Modification

The stability field of the 4H phase dominates Fig. 2. Every value of y and a wide range of x values are encompassed. An unexplained phenomenon is evident in the upper portion of Fig. 2. The nearly parallel isobars within the single phase 4H region slope toward Sr-rich compositions which have progressively smaller x parameters. The conclusion, that at constant temperature Ba-rich 4H phases are slightly more reduced than the Sr-rich 4H phases, seems contrary to expectation. Generally, at a given partial pressure of oxygen and temperature, larger concentrations of the higher oxidation states of a transition metal are stabilized in the presence of the larger Ba^{2+} cation. From the Ba-rich to the Sr-rich end members, Δx values range as high as 0.05 at 1375°C to as low as 0.03 at 1490 and 1610°C. The x-parameters shown in Fig. 2 and listed in Table I are reproducible. They were confirmed by gravimetric studies using: (a) different specimens of the same composition which were given variable and identical thermal treatments; and/or (b) specimens of the same composition which were equilibrated at higher and lower temperatures prior to equilibration at the temperature of interest.

The linear variation of the hexagonal c-parameter as a function of y within the single-phase region of the 4H phase is illustrated for five temperatures in Fig. 7. At a fixed y, cell expansion is evident with increasing temperature (or x). The position of the 10H–4H and 4H–perovskite solvus curves of Fig. 2 are superimposed in Fig. 7 to delimit the extent of the 4H single phase region within the given temperature range. A similar family of lines is derived by plotting the corresponding hexagonal a parameters, listed in Table I, against y. It is possible to rapidly oxidize at 1000°C 4H phases which were prepared in reduced form at elevated temperatures. Cell parameters for these phases are shown in Fig. 8. These parameters are independent of the temperature at which a reduced 4H phase was initially prepared. At $y = 0.60$, for example, reduced 4H forms were prepared at 1225, 1375, 1490, and 1610°C. Although the phase from each temperature has a c parameter which can be determined directly or by interpolation from Fig. 7, oxidation yields a phase with a significantly smaller and constant c (and a) as shown in Fig. 8 and Table I. The linear relationships illustrated in Fig. 8 suggest that rapidly oxidized 4H forms are nearly stoichiometric with respect to anion content. The cell parameters $a \approx 5.45$ Å, $c \approx 9.08$ Å are derived, for example, for the stoichiometric 4H $SrMnO_3$ end member ($y = 1.0$) by a short extrapolation of the lines in Fig. 8. Negas and Roth (*1*, *2*) report $a = 5.449$ Å and $c = 9.078$ Å for 4H $SrMnO_3$. Similarly, Syono et al. (*6*) report $a = 5.449$ Å and $c = 9.085$ Å, while Chamberland

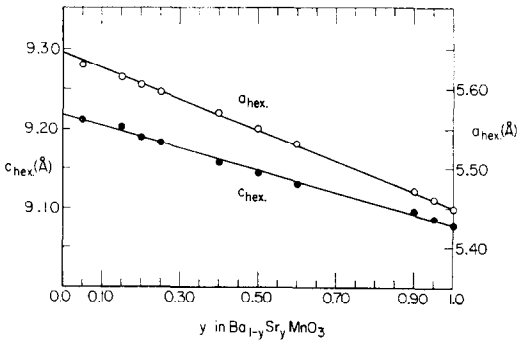

FIG. 8. Variation of the hexagonal cell dimensions at room temperature of 4H phases in the $Ba_{1-y}Sr_yMnO_{3-x}$ system. Specimens were prepared at various temperatures within the single phase 4H field in Fig. 2 and initially were oxygen deficient. These were then oxidized ($x \approx 0$) at 1000°C. Data for 4H $SrMnO_3$ ($y = 1.0$) were taken from Negas et al. (*1*, *2*).

et al. (*7*) report $a = 5.449$ Å and $c = 9.080$ Å. It is apparent from Table I, from the discussion above, and from a comparison of Figs. 7 and 8, that the cell dimensions of oxidized specimens are the smallest which can be derived experimentally. An extrapolation of the lines in Fig. 8 to $y = 0$ therefore yields the parameters $a \approx 5.65$ Å and $c \approx 9.22$ Å which would be predicted for stoichiometric 4H $BaMnO_3$. Syono et al. report $a = 5.645$ Å and $c = 9.264$ Å for a presumably stoichiometric 4H form prepared at 90 kb and 1200°C. Negas and Roth (*3*) report $a = 5.637$ Å and $c = 9.234$ Å for a 4H form which was prepared initially above 1550°C and rapidly oxidized at 500°C in air.

Expansion of the 4H cell as oxygen loss (x) increases suggests that the 4H prototype, $BaMnO_3$, reported by Hardy (*8*) is not stoichiometric. His phase has particularly large parameters, $a = 5.669$ Å and $c = 9.375$ Å. Chamberland et al. (*7*) report a nonstoichiometric, 4H, $BaMnO_{2.85}$ with expanded cell parameters, $a = 5.706$ Å and $c = 9.370$ Å. Negas and Roth (*1*, *3*) report $a = 5.672$ Å and $c = 9.319$ Å for $BaMnO_{\sim 2.75}$, a nonstoichiometric 4H phase, prepared above 1550°C in air. These parameters are in excellent accord with that which would be predicted by extrapolating the 1610°C line in Fig. 7 to the $BaMnO_{3-x}$ ($x \approx 0.27$) end member.

A small orthorhombic distortion of the 4H cell was observed between 1222–1400°C and $0.04 < x < 0.11$ in $SrMnO_{3-x}$ by Negas and Roth (*1*, *2*). This distortion is not evident when as little as 2 mole-% of the larger Ba^{2+} cation is incorporated in solid solution.

Perovskite Phases

Negas et al. (*1*, *2*) showed that at ~1400°C in air reduced 4H $SrMnO_{3-x}$ transforms to a perovskite-like phase with $x > 0.25$. The X-ray powder patterns obtained at room temperature were indexed on the basis of a simple orthorhombic perovskite cell, but it was stressed that the patterns are of extremely poor quality. Although the true symmetry at elevated temperatures could not be deduced, the "perovskites" were converted to a cubic perovskite, characterized by an exceedingly sharp X-ray diffraction pattern, by rapid oxidation to $SrMnO_3$ at temperatures as low as 150°C. The perovskite field extends within the $Ba_{1-y}Sr_yMnO_{3-x}$ system to an experimentally derived value of y as small as 0.90. Values of x range from ~0.25 at 1400°C to ~0.34 at 1610°C. Additions of the larger Ba^{2+} cation to $SrMnO_{3-x}$ increase the temperature of the 4H → perovskite transition from ~1400°C to at least 1610°C. The larger Ba^{2+} cation stabilizes the 4H phase (C/H = 1.0) with respect to the perovskite (C/H = ∞). As y decreases, stabilization of the perovskite phase must be accomplished according to method (b) previously discussed. Greater concentrations of the larger Mn^{3+} cation are required as y decreases. Temperature, therefore, must be raised to promote the reduction process and thereby to induce the 4H → perovskite transition.

The perovskites quenched to room temperature from $y = 0.98$ to 0.95 are similar to those observed in the $SrMnO_{3-x}$ system. Perovskites quenched from $y = 0.93$ and 0.90, however, are cubic. This suggests that the perovskites are probably cubic at high temperature for every relevant value of y. The structure of phases with $y \geq 0.95$ is grossly anion deficient ($x > 0.25$) and apparently collapses when quenched to room temperature. This accounts for the distortions and for the poor crystallinity suggested by their X-ray diffraction powder patterns. With $y < 0.95$ the larger Ba^{2+} cation apparently prevents this collapse. Phases remain cubic when quenched to room temperature, regardless of the anion deficiency. All of the reduced perovskites can be oxidized completely within a few minutes between 150–500°C to yield cubic perovskite phases. The effects of oxidation are illustrated by the portions of X-ray diffraction patterns in Fig. 9 (a, b) and

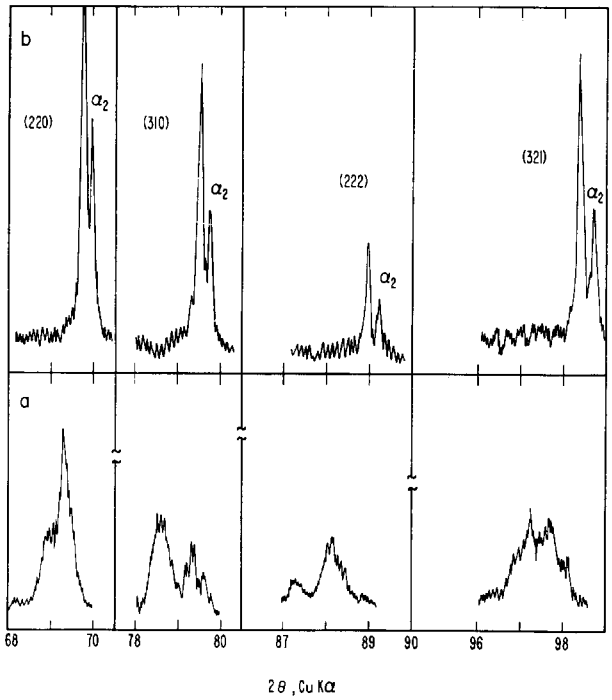

FIG. 9. Portions of the X-ray diffraction powder patterns at room temperature of a perovskite phase prepared at 1610°C and $y = 0.98$ in $Ba_{1-y}Sr_yMnO_{3-x}$. The oxygen-deficient ($x \approx 0.34$), poorly crystalline and distorted form is shown in (a). The cubic pattern in (b) is obtained after the phase in (a) is oxidized ($x \approx 0$) at 400°C (~10 min) in air. The segmented vertical lines are discontinuities along the 2θ scale.

Fig. 10 (a, b). Distorted and/or poorly crystalline perovskites transform to cubic perovskites characterized by high-quality X-ray spectra and smaller cell parameters. The a parameter of phases which were quenched in the cubic form also decreases after oxidation. For example, at $y = 0.90$, a contracts from 3.850 Å to 3.819 Å. Figure 11 shows a linear relationship between a (cubic) and y for oxidized perovskite phases. An a parameter between 3.805–3.807 Å is derived for a stoichiometric $SrMnO_3$ perovskite by extrapolating to $y = 1.0$. Negas et al. (*1*, *2*) report $a = 3.806$ Å for this end member. It is emphasized that the perovskites must be quenched rapidly to room temperature. Oxidation is so rapid that perovskites which are slow-cooled or "air-cooled" will have erroneously high anion contents and possibly false symmetry.

Recently, Mizutani et al. (*13*) independently confirmed the existence of a perovskite field in their $SrMnO_{3-\delta}$ system. They report a reversible 4H ↔ perovskite transition in air at ~1400°C and an oxygen deficiency in the perovskite of $\delta \leqq 0.3$. They also found that the oxygen-deficient perovskites can be oxidized at 300°C to a cubic, stoichiometric, $SrMnO_3$ perovskite with $a = 3.8057$ Å. These data are in excellent agreement with the data of Negas et al. (*1*, *2*) and this study.

Recently, Banks et al. (*14*) reported data which are pertinent to the $Ba_{1-y}Sr_yMnO_{3-x}$ system, especially at large y values. They found that in their $SrFe_yMn_{1-y}O_{3-x}$ system x increased as y increased between 0.4–0.7. Anion-deficient ($x > 0.25$) cubic perovskites are stable within this range. The iron was mostly Fe^{3+} but the manganese was in mixed 3+ and 4+ states. In the $Ba_{1-y}Sr_yMnO_{3-x}$ and $SrMnO_{3-x}$ systems (*1*, *2*) the oxygen deficiency parameter is, indeed, >0.25. Banks et al. also report that a transition to a 4H modification occurs between $y = 0.10$ and $y = 0$. An anion deficiency of $x = 0.11$ was observed. Negas and Roth (*2*) reported this identical value as the stability limit of 4H $SrMnO_{3-x}$. The $SrFe_yMn_{1-y}O_{3-x}$ is thus comparable to the $Ba_{1-y}Sr_yMnO_{3-x}$ and $SrMnO_{3-x}$ systems. The mechanism by which oxygen deficiency is induced differs. Oxygen vacancies are induced at constant temperature in the former system primarily by the substitution of Fe^{3+}.

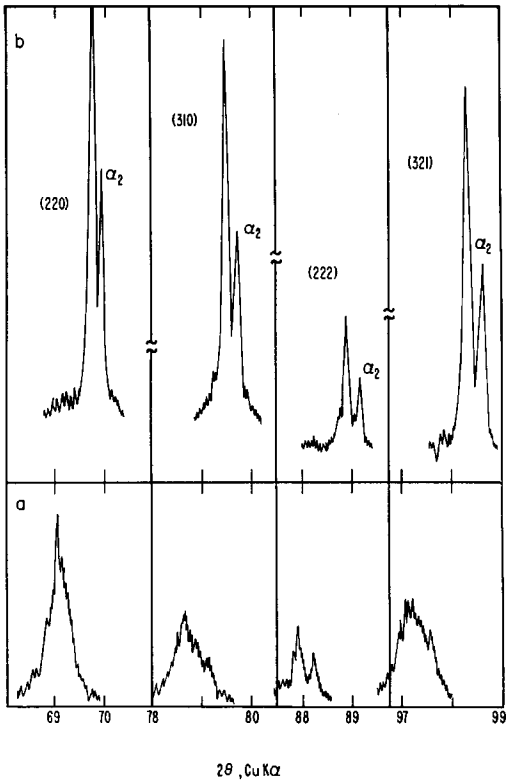

FIG. 10. Portions of the X-ray diffraction powder patterns at room temperature of a perovskite phase prepared at 1610°C and $y = 0.95$ in $Ba_{1-y}Sr_yMnO_{3-x}$. The oxygen-deficient ($x \approx 0.34$), poorly crystalline and distorted form is shown in (a). The cubic pattern in (b) is obtained after the phase in (a) is oxidized ($x \approx 0$) at 400°C (~10 min) in air. The segmented vertical lines are discontinuities along the 2θ scale.

Oxygen losses in the latter systems are the result of reduction of Mn^{4+} to Mn^{3+} as a function of increasing temperature.

Summary

Phase relations in the $Ba_{1-y}Sr_yMnO_{3-x}$ system reflect two competitive processes that tend to stabilize ABO_3 or ABO_{3-x} compounds which have variable "cubic to hexagonal"-type stacking ratios. Increases in the concentrations of (a) the smaller Sr^{2+} cation, and (b) the larger Mn^{3+} cation relative to Mn^{4+}, stabilize phases with progressively larger C/H ratios. Reduction to Mn^{3+} is accomplished by oxygen losses at elevated temperatures. Phases which result are not of fixed anion content (ABO_3) and, therefore, are not related by true polymorphism or polytypism. The view that these phases are simple, oxygen-deficient compounds is strongly supported by gravimetric studies and the expansion of cell parameters as temperature is increased. Furthermore, the anion lattices of reduced phases can be "filled" by oxidation at <1000°C without a major structural change. Reduced phases are characterized by poor-quality X-ray spectra, typical of disordered and/or poorly crystalline materials. Cell dimensions decrease after oxidation. The corresponding X-ray diffraction patterns are of excellent quality, typical of highly ordered, well-crystallized materials. Oxygen diffusion at <1000°C into phases containing vacant anion sites is a simple, rapid process compared with the structural rearrangements which would be required to increase the C/H ratio of any reduced phase (see, for example, the oxidation of the oxygen-deficient perovskites).

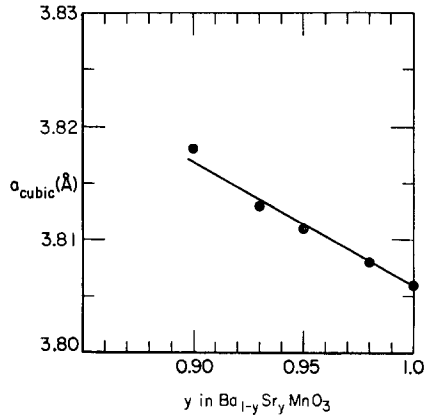

FIG. 11. Variation of the cubic a dimension at room temperature of perovskite phases in the $Ba_{1-y}Sr_yMnO_{3-x}$ system. Specimens were prepared at various temperatures within the single phase perovskite field in Fig. 2 and initially were oxygen deficient ($x > 0.25$). These were then oxidized ($x \approx 0$) at 400°C. Data for the perovskite at $y = 1.0$ ($SrMnO_3$) were taken from Negas et al. (*1*, *2*). See also Figs. 9 and 10.

References

1. T. NEGAS, R. S. ROTH, AND J. L. WARING, Abstract 108, Inorganic Chemistry Division, American Chemical Society, 156th National Meeting (1968).
2. T. NEGAS AND R. S. ROTH, *J. Solid State Chem.* **1**, 409 (1970).
3. T. NEGAS AND R. S. ROTH, *J. Solid State Chem.* **3**, 323 (1971).
4. "International Tables for X-ray Crystallography," Vol. II ,p. 342. Kynoch Press, Birmingham, 1959.
5. L. KATZ AND R. WARD, *Inorg. Chem.* **3**, 205 (1964).

6. Y. Syono, S. Akimoto, and K. Koto, *J. Phys. Soc. Jap.* **26**, 993 (1969).
7. B. L. Chamberland, A. W. Sleight, and J. F. Weiher, *J. Solid State Chem.* **1**, 506 (1970).
8. A. Hardy, *Acta Crystallogr.* **15**, 179 (1962).
9. J. M. Longo and J. A. Kafalas, *Mater. Res. Bull.* **3**, 687 (1968).
10. R. D. Shannon and C. T. Prewitt, *Acta Crystallogr. Sect. B* **25**, 925 (1969).
11. R. D. Burbank and H. T. Evans, *Acta Crystallogr.* **1**, 330 (1948).
12. P. C. Donohue, L. Katz, and R. Ward, *Inorg. Chem.* **4**, 306 (1965).
13. N. Mizutani, N. Ohkuma, A. Kitazawa, and M. Kato, *Kogyo Kagaku Zasshi* **73**, 1103 (1970).
14. E. Banks, O. Berkooz, and T. Nakagawa, NBS Institute for Mater. Res., 5th Mater. Res. Symposium (1971). Abstract, p. 48. Paper to be published.